Advanced Robotics

ISSN: 0169-1864 (Print) 1568-5535 (Online) Journal homepage: http://www.tandfonline.com/loi/tadr20

Fuzzy control-based real-time robust balance for a humanoid robot

Jun-Wei Chang, Rong-Jyue Wang, Che-Han Chang, Hao-Gong Chou & Wen-June Wang

ADVANCED ROBOTICS, 2016
http://dx.doi.org/10.1080/01691864.2016.1202137

FULL PAPER

Fuzzy control-based real-time robust balance for a humanoid robot

Jun-Wei Chang[a], Rong-Jyue Wang[b], Che-Han Chang[c], Hao-Gong Chou[a] and Wen-June Wang[a]

[a]Department of Electrical Engineering, National Central University, Taoyuan City, Taiwan; [b]Department of Electronic Engineering, National Formosa University, Huwei Township, Taiwan; [c]MiTAC Computing Technology Corp., Taipei City, Taiwan

ABSTRACT

This paper studies and implements a real-time robust balance control for a humanoid robot under three environment disturbances which are an external thrust, an inclinable platform, and a see-saw. More precisely to say, the robot with robust control can resist an external thrust, stand on a two-axis inclinable platform, or walk on a see-saw successfully. The main feature of the robot is that it has a waist joint which has three degrees of freedom. With the aids of the proposed fuzzy controllers, the robot can change the posture of the body nimbly by adjusting the waist joint and two ankle joints to strengthen the stabilization capacity. The sensory system of the robot includes eight force sensors and one inertial measurement unit sensor in order to measure the center of pressure and the slant angle of the robot's body. According to the measured data from the sensors and by imitating human reflex actions, the proposed fuzzy controllers perform real-time balance control for the robot under three environment disturbances. According to the experiment results, the stability of the robot is increased at least 32.2 and 61.7% under the first two environment disturbances, respectively. In addition, the robot walking on a see-saw has a success rate of about 95%.

ARTICLE HISTORY
Received 9 February 2016
Revised 3 May 2016
Accepted 6 June 2016

KEYWORDS
Humanoid robot; balance control; fuzzy controller; sensor feedback

1. Introduction

The issue of balance motion control of humanoid robots has been studied by a lot of papers. Some studies [1–5] focused on how to generate stable motion trajectories for a humanoid robot such that the robot can demonstrate certain motions such as walking or dancing. Besides the stable motion design of the humanoid robot, some scholars also consider the problem of the robot's dynamic stability when performing more complex motions. Here, the Zero Moment Point (ZMP) is a point on the ground plane when the total moments of ground contacts equals zero, so that the ZMP concept was employed as a stability index for analyzing the dynamic stability of the humanoid robot. In papers,[6–10] the control strategy was to keep the ZMP in the stability region when the humanoid robot walks. Although the stability of the humanoid robot can be guaranteed in computer simulations, some uncertain perturbations such as hardware limits (backlash and precision errors from the control chip inside the motor), or external disturbances (the friction of the floor and the elasticity of links) may influence the stability of the humanoid robot in practical experiments. It is necessary to measure the feedback data adopted from the sensors of humanoid robot to check its stability. Usually, the center of pressure (CoP) position of the humanoid robot has been used as the dynamic stability index when a humanoid robot performs motions. Papers [11,12] studied the relationship between the CoP and the stability of the robot and focused on how to make the humanoid robot walk stably on a horizontal floor or in a safe environment without any uncertainty.

When a biped robot stands or walks in a real ground, generally, we may concern two situations. One is whether the robot can maintain its balance when it is pushed by an external force, and the other is whether the robot can walk stably even the ground is titled or moving. Therefore, many studies have investigated the balance control for a humanoid robot under various environment disturbances. The authors of [13] used the measured data from the force sensors as the controller input to adjust the robot's posture such that the humanoid robot can walk on a slanted floor successfully. In fact, many papers have studied the problem of how a humanoid robot can maintain dynamic balance by overcoming external disturbances such as thrusts [14,15], movable platforms [16,17], and slanted floors [18,19].

CONTACT Rong-Jyue Wang orffwang@nfu.edu.tw

In the paper,[8] the humanoid robot has a spine structure with 3-DOF joints to maintain real-time balance using a hybrid CPG–ZMP controller so that the robot is much nimbler than many other robots to overcome external disturbance. In the paper,[11] a six-axes force–torque sensor was developed and a dynamically stable gait pattern was generated to make the robot walk on unstructured terrain successfully. The robot in the paper [12] is a biped robot without upper body and the torso correction of the robot's body is applied to ensure walking stably and resist thrusts from the front and the rear (lateral thrusts are not included). A learning capture points technique was proposed by [14] in which the robot takes a step to recover the push effect. The paper [15] proposed a new force control framework which control ground applied force without inverse kinematics to against the external pushing forces. Kinematic synergies inspired from biology were used in [16] to help the robot being able to stand and keep balance on a tilted plane. By controlling the desired ground reaction force (GRF) and center of pressure (CoP) at each support foot, the humanoid robot can maintain its balance under external thrust and on an inclinable platform.[17] The authors of [18] designed a motion control method to adjust the center of gravity of the biped robot inside the convex region of the supporting feet when the robot walks on a specific slope. The robot maintains postural balance using an observer-based balancing control strategy to estimate the ground slope is proposed in [19]. The paper [20] adopted adaptive neural fuzzy networks to cancel perturbations and H_∞ tracking to attenuate external disturbance for a human-like walking robot.

In this study, we try to use fuzzy rules to establish robust controllers for a humanoid robot such that the robot can resist an external thrust, stand on a two-axis moving inclinable platform, or walk on a see-saw, respectively. Two aspects are combined to overcome the disturbances, one is the hardware aspect and the other is the software aspect. In the hardware aspect, we add a joint consisting of three degrees of freedom in the waist position of the humanoid robot and use some sensors to measure the posture of the robot. In the software aspect, we propose a complete fuzzy control strategy for the humanoid robot to deal with the aforementioned three disturbances. Finally, this paper provides a series of experiments to verify the efficiency of the proposed controller strategy. The experimental data show that the robot is significantly more stable at least 32.2 and 61.7% when the robot encounters the first two disturbances, respectively. In addition, the success rate of walking on the see-saw is about 95%.

Comparing to the previous papers [8,11,14,15,17,19], this study proposes a more effective real-time control and performs the control on a real humanoid robot actually. Since the papers [8,17] only provided the simulation results without real experiments. The papers [14,15] only considered to overcome the situation of external thrust. The robot walking only on an even ground was considered in [11]. In paper [19], the robot stands on an inclinable platform whose slope is with only one axis. Moreover, it should be emphasized that a robot walking on a see-saw is a novel study which is seldom found in other literatures.

This paper is organized as follows. Section 2 presents a description of the hardware structure. Section 3 introduces natural human reactions for resisting external disturbances. Section 4 provides a real-time balance control for the robot. Section 5 demonstrates the experimental results. The conclusion is given in the final section.

2. Description of the hardware structure

The hardware structure of the humanoid robot system is comprised of four parts: the robot's body, a small computer RoBoard RB-100, a Razor Inertial Measurement Unit (IMU) sensor module, and eight force sensor modules as shown in Figure 1. The robot's body is constructed on the basis of 22 AX-12 motors with some plastic links as shown in Figure 2. The weight and height of the robot are about 2 kg and 42 cm, respectively. The robot has 22 degrees of freedom (DoFs) in total as shown in Figure 3. For convenience, the robot was named 'CU-robot.'

The RoBoard RB-100 [21] is a small, light computer which is usually used as the control center of small humanoid robots. The Razor IMU module,[22] which, when set on an object, can measure the object's slant angles on X–Y–Z axes. The IMU sensor module is placed just above the robot's hip as shown in Figure 2, then the slope angles (α and β) of the robot's upper body in the Y–Z and X–Z planes can be measured as in Figure 4(a) and (b), respectively. There is a force sensor module [23] installed on each of the four corners of both soles of the robot, so that the pressure of each corner can be measured.

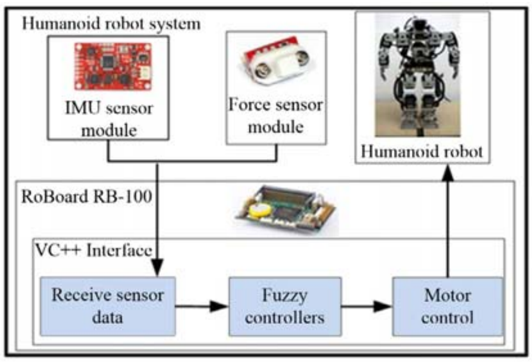

Figure 1. The structure of the humanoid robot system.

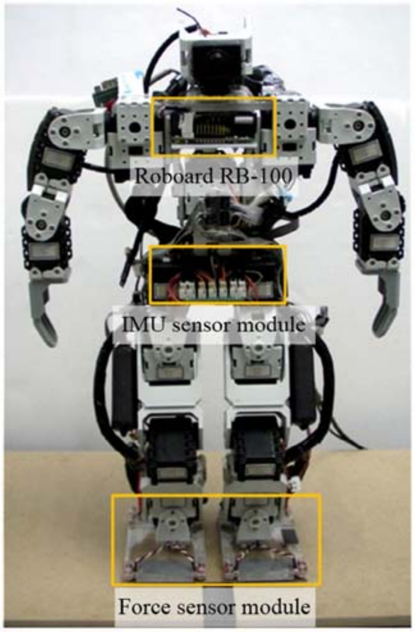

Figure 2. The humanoid robot (CU-robot).

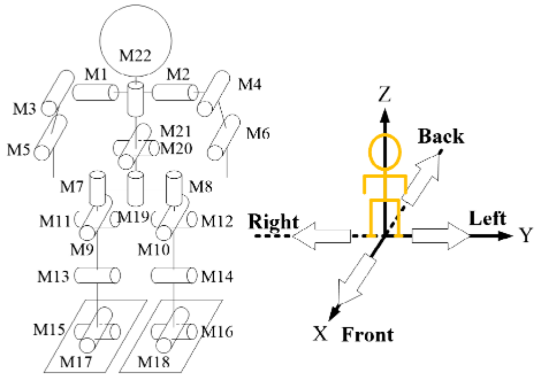

Figure 3. DoFs of the CU-Robot.

The structure of the CU-robot is similar to that of the Bioloid robot,[24] but the waist joint has been redesigned for the CU-robot, and the RB-100 and IMU sensor module are set on the upper body of the CU-robot. Thus, if the CU-robot imitates the walking posture of the Bioloid robot completely, it would fall down due to the unsuitable slope angle of robot's upper body (see Figure 5(a), $\theta_{\text{body}} = 12°$ from [24]. Because, the upper body of the CU-robot is much heavier than that of the Bioloid robot, the slope angle of the upper body needs to be adjusted (by rotating motors $M11$ and $M12$ in Figure 3) according to the CoP position as measured by the force sensor module to maintain the robot's stability while walking. In our experiments, when the CU-robot walks forward, or backward, the slant angles of its upper body are fixed at $\theta_{\text{body}} = 2°$ and $\theta_{\text{body}} = 7°$ as shown in Figure 5(b) and (c), respectively.

3. Analysis of natural human reflex actions

In order to effectively adjust the waist and ankle joints of the CU-robot to maintain stability, the reactive motions of the CU-robot are designed based on the natural reflex actions of a human. According to the references [14–16] and observations of real humans, the reflex actions which conquer external disturbances will be introduced, including an external thrust from a hammer, a two-axis inclinable platform, and a see-saw. The reflex actions can be separated into two conditions as follows.

3.1. Condition I: When a disturbance approaches from the front or rear of a human (Pitch case)

When a disturbance approaches from the front or rear of a human body, the human usually changes their upper body posture to relocate their CoP to a safe region by adjusting their waist joint, and keeps their lower body vertical to the ground (the degree of β (see Figure 4(b)) is close to zero) by adjusting their ankle joints, so that

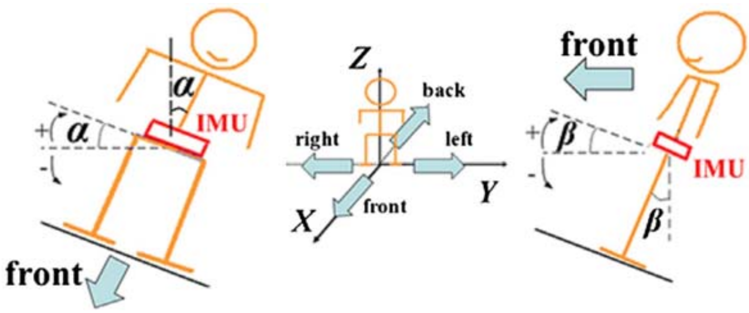

Figure 4. (a) The slope angle α of the robot on the Y–Z plane. (b) The slope angle β of the robot on the X–Z plane.

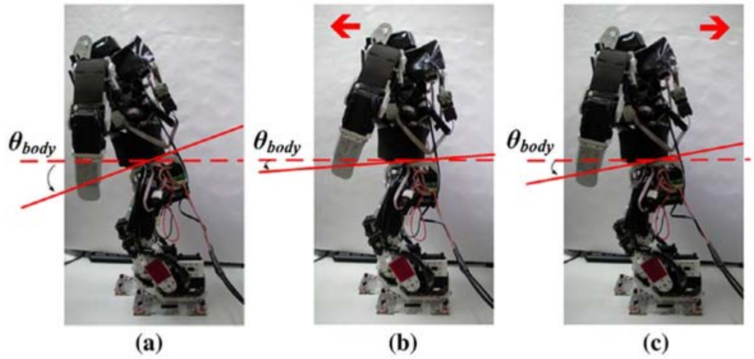

Figure 5. (a) The walking forward posture of the Bioloid robot.[24] (b) The walking forward posture of the CU-robot. (c) The walking backward posture of the CU-robot.

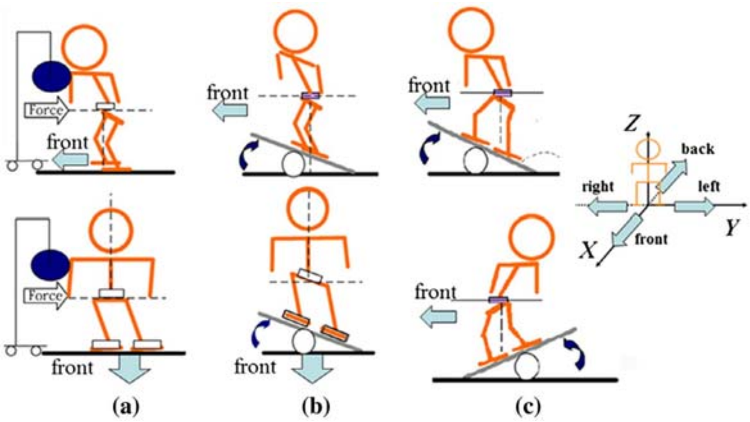

Figure 6. (a) Resisting an external thrust. (b) Standing on a two-axis inclinable platform. (c) Walking on a see-saw.

they can maintain balance to defend against the thrust or stand on the sloping platform without falling down as shown in the upper parts of Figure 6(a) and (b). Using the same reflex strategy as above, when a human walks on a see-saw from one terminal to the other as shown in Figure 6(c), they also adjust their ankle and waist joints to walk on the see-saw stably.

3.2. Condition II: When a disturbance comes from the lateral side of a human (Roll case)

When a disturbance comes from the lateral side of a human, the human usually keeps their upper body vertical to the ground (the degree of α (see Figure 4(a)) is close to zero) by adjusting their waist joint and changes their lower body posture by adjusting their ankle joints to relocate their CoP to a safe region, so that they can maintain balance and stand on the ground or the sloping platform without falling down as shown in the lower parts of Figure 6(a) and (b).

The concept of the above natural human reflex actions will be applied to the CU-robot such that it can resist the above three external disturbances by adjusting both ankle and waist joints at the same time in the next section.

4. A real-time balance control for the CU-robot

In this section, a real-time balance control that allows the CU-robot to overcome external disturbances will be designed. A disturbance can make the CU-robot fall down easily if the robot does not have controllers to adjust its posture to defend against the disturbance in real time. Therefore, some information such as the CoP of the robot and the slope angles of the robot's body measured from the force sensor modules and IMU sensor should be employed as the stability indices of the robot for the purpose of controller design. Here, two kinds of fuzzy controllers for adjusting the ankles and waist, respectively, will be proposed to conquer the external disturbances.

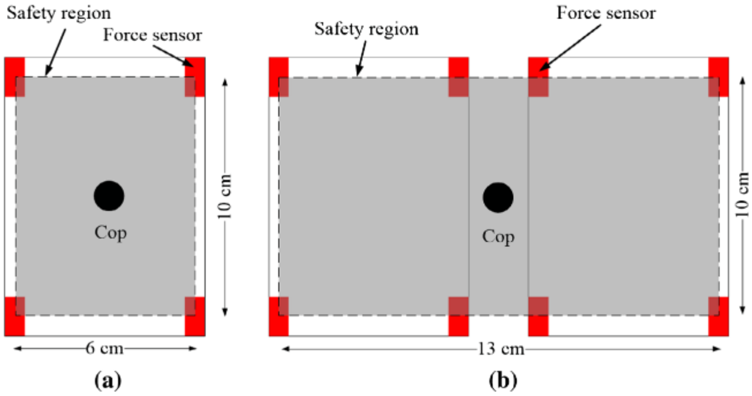

Figure 7. (a) The safe region of the SSP. (b) The safe region of the DSP.

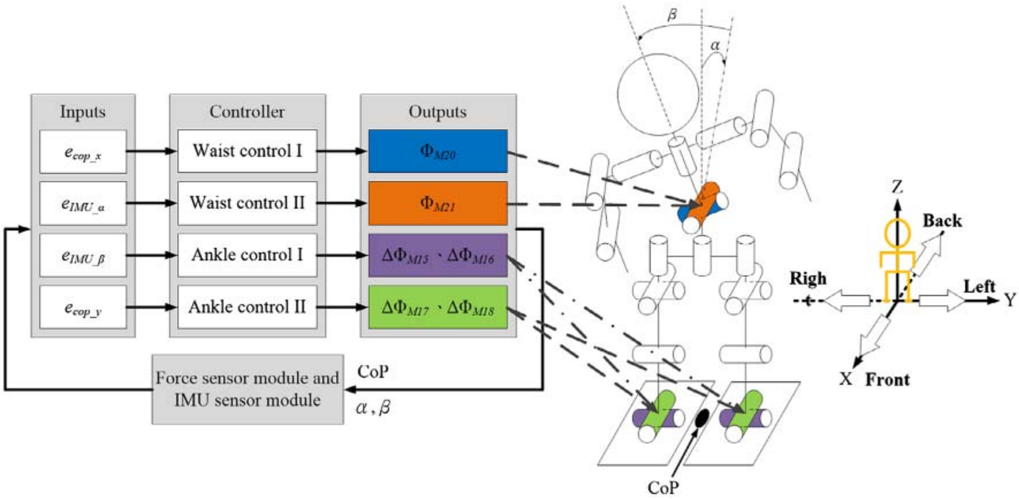

Figure 8. The fuzzy controllers for adjusting the ankles and waist.

4.1. Two kinds of inputs for the fuzzy controllers

In general, the slope angles and the CoP position of a humanoid robot are chosen as the stability indices. The slope angles such as α and β in Figure 4 of the CU-robot can be measured by the IMU sensor in the hip. The two angles are used to check whether the upper or lower body of the robot is vertical to the ground. The CoP position can be calculated from the measured pressure at the four corners of each robot's sole. The CoP plays a key role in the stability of the robot. If the CoP position is outside the 'safe region,' the robot will fall down.[11] When the humanoid robot stands on the ground on a single foot, the safe region is defined as the area of the sole. Then, the robot is in a single support phase (SSP) as shown in Figure 7(a). In an SSP, the CoP position (x_c, y_c) is calculated from by (1) with $n = 4$,

$$\text{CoP} = \frac{\sum_{i=1}^{n} F_i \cdot d_i}{\sum_{i=1}^{n} F_i} \quad (1)$$

where F_i is the pressure value measured from the i-th sensor, and d_i is the vector from the CoP to the i-th sensor. When the robot stands on two feet, it is in a double support phase (DSP) as shown in Figure 7(b). In a DSP, the CoP position of the robot can also be calculated from (1) with $n = 8$. The above two stability indices (the slope angle and the CoP position of the CU-robot) will be given as inputs to the fuzzy controllers for adjusting the ankles and waist, respectively, and will be introduced in the next subsection.

4.2. Fuzzy controllers for adjusting the ankles and waist

In Figure 8, the CU-robot is standing and facing along the X-axis as shown on the right side of the figure, where Φ_{Mi} denotes the rotation degree of the motor Mi. If the slope angle of the robot is not at the desired degree or the CoP position is outside the safe region, the controllers would simultaneously adjust Φ_{M20} and Φ_{M21} in the waist joints (see Figure 3) and Φ_{M15} to Φ_{M18} in the ankle joints (see Figure 3) on the X–Z and Y–Z planes, respectively, to maintain the robot's stability and maintain its desired body posture. Therefore, let the error of slope angles (e_{IMU_α}, e_{IMU_β}) and the error of CoP position (e_{cop_x}, e_{cop_y}) measured from the IMU and force modules in the X–Z and Y–Z planes be the inputs of the fuzzy controllers for adjusting the ankles and waist to make the robot stably and maintain its desired body posture. Here, (e_{IMU_α}, e_{IMU_β}) is the angle error between the slope angle (α and β) and the desired degree. When the CU-robot stands on the ground or the inclinable platform, e_{IMU_α} and e_{IMU_β} are equal to α and β (the desired degree is zero). When the CU-robot walks on a see-saw from one terminal to the other, e_{IMU_α} is still equal to α, but e_{IMU_β} is changed to $e_{IMU\_\beta} = \beta - \theta_{forward}$ (walk forward) or $e_{IMU\_\beta} = \beta - \theta_{backward}$(walk backward) as shown in Figure 5(b) and (c). Next, (e_{cop_x}, e_{cop_y}) is the position error between the current CoP and the center of safe region.

The fuzzy controllers for adjusting the ankle and waist include four fuzzy controllers which are Waist Control I, Ankle Control I, Waist Control II, and Ankle Control II (see Figure 8). Waist Control I and II are used for controlling the rotation degrees of $M20$ and $M21$, respectively. Ankle Control I and II are for controlling the rotation degrees of ($M15$, $M16$) and ($M17$, $M18$), respectively. Therefore, when the disturbance affects the robot, the corresponding controllers perform. In the following, we will explain how the controllers perform to resist the external disturbances.

4.2.1. When a disturbance comes from the front or rear of the robot (Condition I in Section 3 (for pitch))

When the external disturbances occur on the front or rear of the robot (Pitch case), Waist Control I adjusts Φ_{M20} (the waist joint rotating on the X–Z plane) and Ankle Control I adjusts $\Delta\Phi_{M15}$ and $\Delta\Phi_{M16}$ ($\Delta\Phi_{M16} = -\Delta\Phi_{M15}$, the ankle joints rotating on the X–Z plane) according to the inputs e_{cop_x} and e_{IMU_β} to maintain the robot's stability and its desired body posture, respectively.

4.2.1.1. Waist Control I for Condition I in Section 3 (for pitch). When Condition I happens, the robot needs to bend its upper body forward or backward to maintain balance intuitively. Therefore, let the CoP position error in the X direction (e_{cop_x}) be chosen as the input of Waist Control I and the motor $M20$ rotation degree in the X–Z plane (Φ_{M20}) is the control output. The center of the safe region of the robot is denoted by CoP_{safe} and CoP_{safe_x} (CoP_{safe_y}) is the component on the X-axis (Y-axis) of CoP_{safe}. It is known that if the X-axis component of the current CoP x_c is near CoP_{safe_x}, then the robot is balanced stably. Otherwise, the robot might fall forward or backward. Let the CoP error on the X-axis (e_{cop_x}) is defined as (2)

$$e_{cop\_x}(s) = \text{CoP}_{safe\_x} - x_c(s) \tag{2}$$

where s is the sampling time. When the e_{cop_x} in (2) is applied to Waist Control I, the output adjusts the rotation degree Φ_{M20} of $M20$ in real time such that the CoP remains inside the safe region. Therefore, we establish a fuzzy rule base for Waist Control I as Table 1, where the premise fuzzy set e_{cop_x} and the consequent fuzzy set ϕ_{M20} are shown in Figures 9 and 10, respectively.

Using a minimum inference engine and center of gravity defuzzification, the final angle Φ_{M20} can be calculated by (3).

$$\Phi_{M20}(s) = \frac{\sum_{i=1}^{10} \phi_{M20}(s) \times h_i(e_{cop\_x}(s))}{\sum_{i=1}^{10} h_i(e_{cop\_x}(s))} \tag{3}$$

where $h_i(e_{cop\_x}(s))$ is the membership degree of the premise fuzzy set e_{cop_x} in rule-i and s is the sampling time. Therefore, based on the rules as in Table 1 and (3), x_c will be moved toward CoP_{safe_x} to increase the stability.

Table 1. Rule table of Waist Control I.

If e_{cop_x} is	NB	NMB	NM	NMS	NS	ZO	PS	PMS	PM	PB
Then φ_{M20} is	PB	PMB	PM	PMS	PS	ZO	NS	NMS	NM	NB

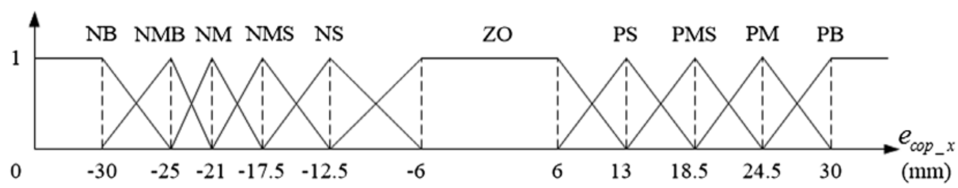

Figure 9. Premise fuzzy sets of e_{cop_x}.

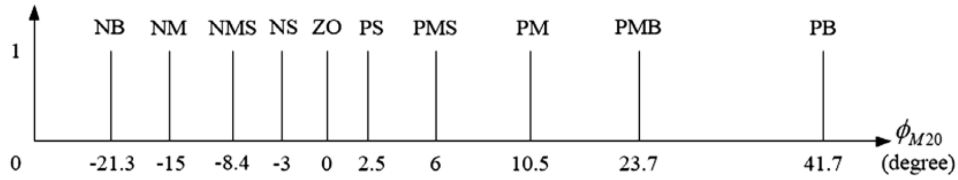

Figure 10. Consequent fuzzy sets of ϕ_{M20}.

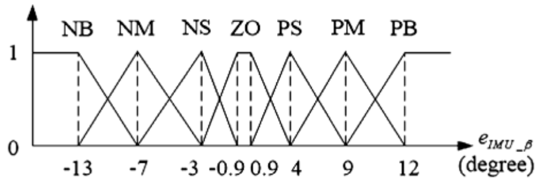

Figure 11. Premise fuzzy sets of e_{IMU_β}.

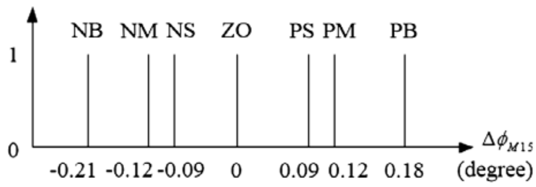

Figure 12. Consequent fuzzy sets of $\Delta\phi_{M15}$.

4.2.1.2. Ankle Control I for Condition I in Section 3 (for pitch). When Condition I happens, the robot needs to adjust its ankle joints to keep the lower body vertical to the ground. Therefore, the slope angle error e_{IMU_β} of the robot's upper body in X–Z plane measured by the IMU is chosen as the input of Ankle Control I and the motors $M15$ and $M16$ rotation degrees in X–Z plane ($\Delta\Phi_{M15}$ and $\Delta\Phi_{M16}$) are the output of the controllers. In other words, Ankle Control I can reduce $|e_{IMU\_\beta}|$ by adjusting the ankle joints (Φ_{M15} and Φ_{M16}, rotating on the X–Z plane) of the robot in real time. The premise fuzzy set e_{IMU_β} and the consequent fuzzy set $\Delta\phi_{M15}$ are shown in Figures 11 and 12, respectively. The rule table of Ankle Control I is shown in Table 2. Using the same inference engine and defuzzification as (3), the $\Delta\Phi_{M15}$ is calculated by (4)

$$\Delta\Phi_{M15}(s) = \frac{\sum_{i=1}^{7} \Delta\phi_{M15}(s) \times h_i(e_{IMU\_\beta}(s))}{\sum_{i=1}^{7} h_i(e_{IMU\_\beta}(s))} \quad (4)$$

Table 2. Rule table of Ankle Control I.

If e_{IMU_β} is	NB	NM	NS	ZO	PS	PM	PB
Then $\Delta\varphi_{M15}$ is	PB	PM	PS	ZO	NS	NM	NB

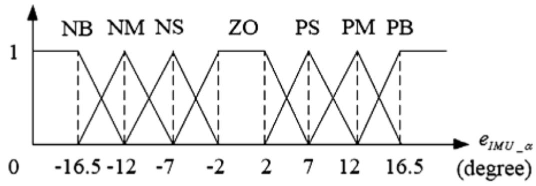

Figure 13. Premise fuzzy sets of e_{IMU_α}.

where $h_i(e_{IMU\_\beta}(s))$ is the membership degree of the premise fuzzy set e_{IMU_β} in rule-i. The final ankle angles on the X–Z plane are $\Phi_{M15}(s+1) = \Phi_{M15}(s) + \Delta\Phi_{M15}(s)$ and $\Phi_{M16}(s+1) = -\Phi_{M15}(s+1)$. Therefore, using Ankle Control I, $|e_{IMU\_\beta}|$ is reduced to as close to zero as possible to keep the robot's lower body vertical to the ground.

4.2.2. When a disturbance comes from the lateral side of the robot (Condition II in Section 3 (for Roll))

When the external disturbances occurs on the lateral side of the robot (Roll case), Waist Control II adjusts Φ_{M21} (the waist joint rotating on the Y–Z plane) and Ankle Control II adjusts $\Delta\Phi_{M17}$ and $\Delta\Phi_{M18}$ ($\Delta\Phi_{M18} = \Delta\Phi_{M17}$, the ankle joints rotating on the Y–Z plane) according to the inputs e_{IMU_α} and e_{cop_y} to maintain the robot's stability and its desired body posture, respectively.

4.2.2.1. Waist Control II for Condition II in Section 3. When Condition II happens, the robot needs to bend its upper body left or right to keep its upper body vertical to the ground. Therefore, let the slope angle error e_{IMU_α} of the robot's upper body in Y–Z plane measured by the IMU be chosen as the input of Waist Control II and the motor $M21$ rotation degree in Y–Z plane (Φ_{M21}) is the control output. In other words, Waist Control II can reduce the $|e_{IMU\_\alpha}|$ by adjusting the waist joint (Φ_{M21}, rotating on the Y–Z plane) of the robot in real time. The premise fuzzy set e_{IMU_α} and the consequent fuzzy set ϕ_{M21} are shown in Figures 13 and 14, respectively. The rule table is the same as Table 2, when the premise fuzzy

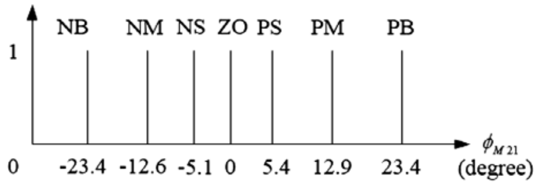

Figure 14. Consequent fuzzy sets of ϕ_{M21}.

set e_{IMU_β} and consequent fuzzy set $\Delta\varphi_{M15}$ are replaced by e_{IMU_α} and ϕ_{M21}, respectively. Using the same inference engine and defuzzification as (3), the final angle Φ_{M21} is calculated by (5).

$$\Phi_{M21}(s) = \frac{\sum_{i=1}^{7} \phi_{M21}(s) \times h_i(e_{IMU\_\alpha}(s))}{\sum_{i=1}^{7} h_i(e_{IMU\_\alpha}(s))} \tag{5}$$

where $h_i(e_{IMU\_\alpha}(s))$ is the membership degree of the premise fuzzy set e_{IMU_α} in rule-i. Therefore, based on the rules as in Table 2 and (5), $|e_{IMU\_\alpha}|$ is reduced to as close to zero as possible to keep the robot's upper body vertical to the ground.

4.2.2.2. Ankle Control II for Condition II in Section 3. When Condition II happens, the robot needs to adjust its ankle joints to move the CoP toward the center of the safe region as soon as possible in Y–Z plane. Therefore, the CoP position error in the Y direction (e_{cop_y}) is chosen as the control input and the motors $M17$ and $M18$ rotation degrees in Y–Z plane ($\Delta\Phi_{M17}$ and $\Delta\Phi_{M18}$) are the output of the controller. It is known that if the Y-axis component of the current CoP y_c is near CoP_{safe_y}, then the robot is balanced stably. Otherwise, the robot might fall left or right. Let the CoP error on the Y-axis (e_{cop_y}) is defined as (6).

$$e_{cop\_y}(s) = \text{CoP}_{safe\_y} - y_c(s) \tag{6}$$

where s is the sampling time. When the e_{cop_y} in (6) is applied to the Ankle Control II, the output adjusts the rotation degrees Φ_{M17} and Φ_{M18} of the motors $M17$ and $M18$ in real time such that the CoP remains inside the safe region. The premise fuzzy set e_{cop_y} and the consequent fuzzy set $\Delta\phi_{M17}$ are shown in Figures 15 and 16, respectively. The rule table of Ankle Control II is the same as Table 2 when the premise fuzzy set e_{IMU_β} and consequent fuzzy set $\Delta\phi_{M15}$ were replaced by e_{cop_y} and $\Delta\phi_{M17}$, respectively. Using the same inference engine and defuzzification as (3), the variation of the ankle angle $\Delta\Phi_{M17}$ was calculated as (7).

$$\Delta\Phi_{M17}(s) = \frac{\sum_{i=1}^{7} \Delta\phi_{M17}(s) \times h_i(e_{cop\_y}(s))}{\sum_{i=1}^{7} h_i(e_{cop\_y}(s))} \tag{7}$$

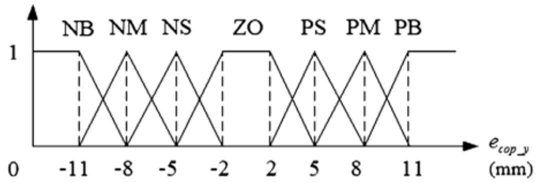

Figure 15. Premise fuzzy sets of e_{cop_y}.

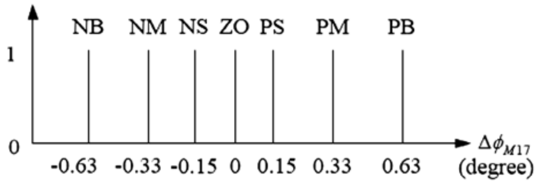

Figure 16. Consequent fuzzy sets of $\Delta\phi_{M17}$.

where $h_i(e_{cop\_y}(s))$ is the membership degree of the premise fuzzy set e_{cop_y} in rule-i. The final ankle angles on the Y–Z plane were $\Phi_{M17}(s+1) = \Phi_{M17}(s) + \Delta\Phi_{M17}(s)$ and $\Phi_{M18}(s+1) = \Phi_{M17}(s+1)$. Therefore, based on Ankle Control II, y_c will be moved toward CoP_{safe_y} to increase the stability. However, the lateral body of the robot is inevitably tilted due to the motors $M17$ and $M18$ rotation. In order to compensate the lateral body tilt, the motors $M9$ and $M10$ will be set to rotate in the opposite direction of $M17$ and $M18$. The main intention to compensate the body tilt is to make the reflex actions of the robot more similar to that of human beings. Based on the $M17$ and $M18$ rotation degree, the compensation of the motors $M9$ and $M10$ rotation degrees are calculated as (8)

$$\begin{aligned} \Delta\Phi_{M9}(s) &= -\Delta\Phi_{M17}(s) \\ \Delta\Phi_{M10}(s) &= -\Delta\Phi_{M18}(s) \end{aligned} \tag{8}$$

In the above description, we have explained the four fuzzy controllers which are used in this paper. It is noted that the parameter values of all the fuzzy sets are adjusted based on the user's experience during the experimentation process. Considering that the RoBoard PB-100 is installed on back of the CU-robot, the weight of the robot's back is greater than that of its front. When the robot is in danger of falling backward, it should more delicately adjust the upper body posture of the robot. Hence, as shown in Figure 9, we arrange the fuzzy sets on the premise part in asymmetrical form, such as five fuzzy sets at the left of ZO and four fuzzy sets at the right of ZO. Furthermore, the supports of those fuzzy sets at the right side are wider than those at the left side. Consequently, based on Table 1, for the consequent part, the distance between any two adjacent singleton fuzzy sets at the right side is larger than that at the left side. On the other hand, the robot's weights on both lateral sides are symmetrical, so that the fuzzy sets of the Ankle Control II and Waist Control II can be designed symmetrically.

Regarding the adjustment of the parameter values, some criterions should be followed to obtain fast the parameter of the fuzzy set. First, the order of the modification of the fuzzy controller parameter must be determined. Since both the Ankle Control II and Waist Control I can adjust the CoP position of the robot on *X*-axis, there will affect each other when the fuzzy set parameters of the two controllers are modified. Besides, the center of gravity of the robot is close to the IMU sensor module. Using the ankle to adjust the CoP position will be more effective. Therefore, the parameter of Ankle Control II should be determined first, and those values must be smaller than 1°, since the ankles are at the bottom of the robot. When the values of Ankle Control II are too larger, the CoP will be outside of the safety region. Then, the parameter of the Waist Control I is assigned and its output should be larger than that of the measured IMU values, since the weight of the robot's upper body is slighter than that of the whole body. Then, the centers of the fuzzy sets are distributed with equal interval. Through a few experiments, the suitable parameters of these fuzzy controllers are obtained. Similarly, the parameter of Ankle Control I and Waist Control II can be modified by the same procedure.

5. Experiment results

In this section, three experiments will demonstrate that the CU-robot with the proposed fuzzy controllers can resist an external thrust, stand on a two-axis inclinable platform, or walk on a see-saw successfully. A video of the three main experiments which shows the experimental effectiveness can be downloaded from [25].

5.1. Resisting an external thrust

In the first experiment, the main purpose is to measure the maximum external thrust force which the robot can overcome with the fuzzy controllers and to verify the fuzzy controller's efficiency. Here, the robot is required to stand straight on flat ground and to resist an external thrust force from a movable hammer platform. The procedure of this experiment is described as follows. First, the entire hammer platform is moved forward slowly by hand until the hammer touches the front, back, or lateral side of the CU-robot. Next, the platform is moved further forward to increase the thrust force of the hammer. Finally, when the robot's soles slide or the robot's feet are no longer touching the ground, the platform is stopped and is then moved backward slowly to decrease the thrust force. The movable hammer platform is shown in Figure 17(a) where the thrust force can be measured by a sensor. When the hammer meets resistance such as a hand (or an obstacle), then the sensor detects the thrust force as shown in Figure 17(b).

To compare the effectivity of the results, we evaluate the performance of each experiment using Equation (9).

$$\eta_f = \left(\frac{F_{on}}{F_{off}} - 100\% \right) \tag{9}$$

in which η_f is the increased stability. F_{on} is the maximum resisted external force when controllers are on; F_{off} is the maximum resisted external force when controllers are off.

5.1.1. An external thrust comes from the front or rear of the CU-robot

When the hammer pushes the front of the CU-robot without any controller, the robot falls down at 3.25 s when the thrust force is 4.1 kgf cm (see the dotted curve in Figure 18(a)). On the other hand, the CU-robot which has Ankle Control I and Waist Control I can resist around 6.2 kgf cm of thrust force (see the solid curve in Figure 18(a) at 17.5 s) and still maintain its balance without falling down. The data of e_{cop_x}, Φ_{M20}, e_{IMU_β}, $\Delta\Phi_{M15}$, and Φ_{M15} during the experiment are shown in Figure 18(b)–(f), respectively. When Waist Control I and Ankle Control

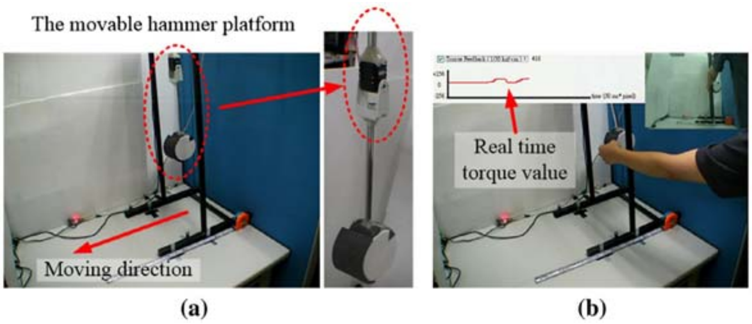

Figure 17. (a) The movable hammer platform. (b)The real-time torque value measurement.

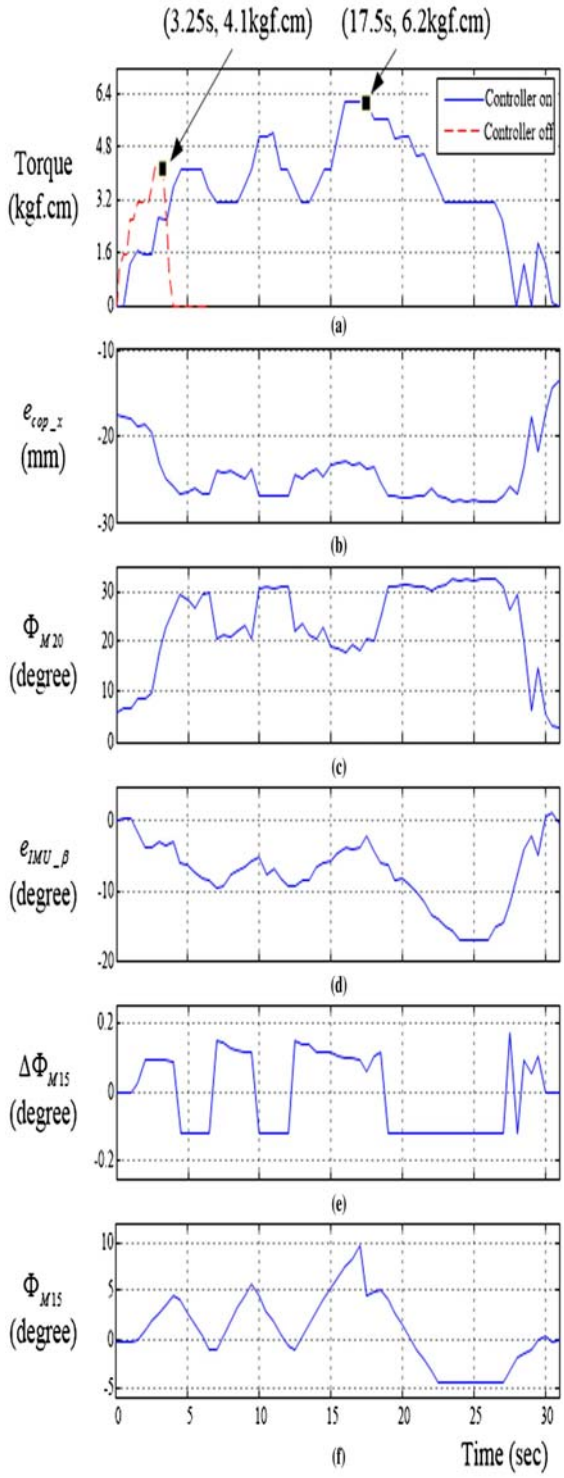

Figure 18. Experimental data when the hammer pushes the front of the CU-robot.

I are used to adjust the waist angle Φ_{M20}, and the ankle joints Φ_{M15} and Φ_{M16}, respectively. e_{cop_x} is kept within the stable interval [−27, −14 mm] (the stable region of e_{cop_x} is [−50, 50 mm] (see Figure 7)) and the CU-robot is able to keep its lower body vertical to the ground. Figure 18(d) shows that the e_{IMU_β} is kept within the interval [−17°, 1°].

When the hammer pushes the back of the CU-robot without any controller, the robot falls down at 3.75 s and the thrust force is 3.1 kgf cm (see the dotted curve in Figure 19(a)). On the other hand, when the Ankle Control I and Waist Control I are applied in this case simultaneously, the CU-robot could resist around 4.1 kgf cm of thrust force (see the solid curve in Figure 19(a) at 19 s) and still keeps its balance without falling down. The data of e_{cop_x}, Φ_{M20}, e_{IMU_β}, $\Delta\Phi_{M15}$ and Φ_{M15} during the experiment are shown in Figure 19(b)–(f), respectively. In this experiment, the e_{cop_x} and e_{IMU_β} are kept within the interval [−5, 35 mm] and [−6°, 8°], respectively. By (9), when the thrust force comes from the front, the increased stability is 51.2%; when the thrust force comes from the rear, the increased stability is 32.2%.

5.1.2. An external thrust comes from the lateral side of the CU-robot

When the hammer pushes the CU-robot laterally without any controller, the robot falls sideways at 6.75 s when the thrust force is 11.9 kgf cm (see the dotted curve in Figure 20(a)). On the other hand, the CU-robot which is using Ankle Control II and Waist Control II can resist a thrust force of around 16.5 kgf cm (see the solid curve in Figure 20(a) at 10.5 s) and still remain balanced without falling down. The data of e_{cop_y}, Φ_{M21}, e_{IMU_α}, $\Delta\Phi_{M17}$, and Φ_{M17} during the experiment are shown in Figure 20(b)–(f), respectively. When Ankle Control II and Waist Control II are applied in this case simultaneously to adjust the ankle joints Φ_{M17} and Φ_{M18}, and the waist joint Φ_{M21}, respectively, e_{cop_y} is kept within the stable interval [−23, 18 mm] (the stable region of e_{cop_y} is [−65, 65 mm] (see Figure 7)) and the CU-robot maintains its upper body vertical to the ground. Figure 20(e) shows that the e_{IMU_α} is kept within the interval [−16°, 7°]. The increased stability of that the thrust force comes from the lateral side is 38.6%. Photographs of the CU-robot resisting an external thrust during the experiment are shown in Figure 21 and the video [25].

5.2. Standing on a two-axis inclinable platform

In the second experiment, the main purpose is to measure the maximum incline angle of the movable two-axis platform at which the CU-robot with the controllers can

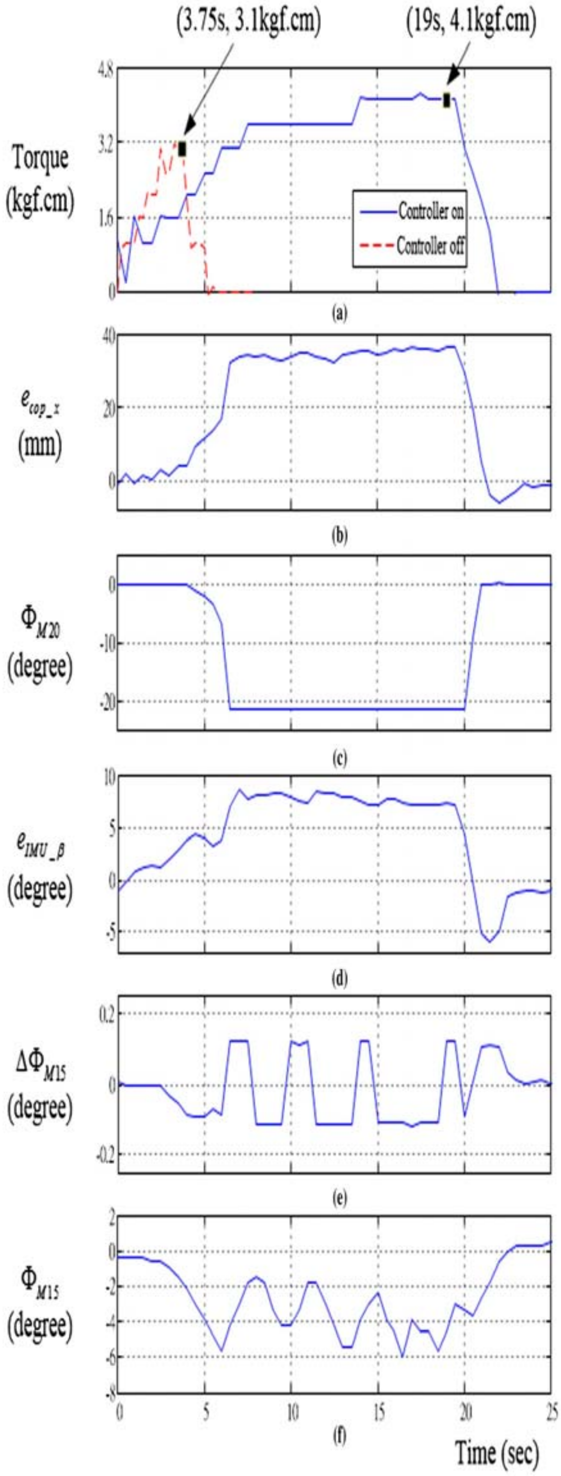

Figure 19. Experimental data when the hammer pushes the back of the CU-robot.

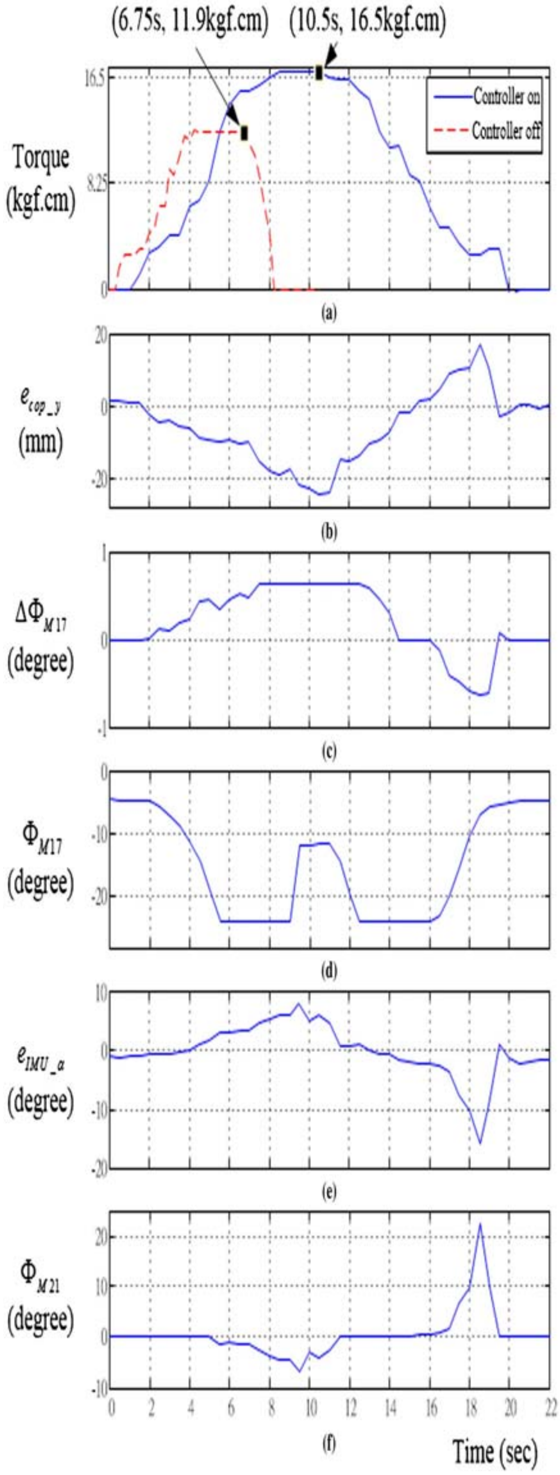

Figure 20. Experimental data when the robot was pushed laterally (from the side).

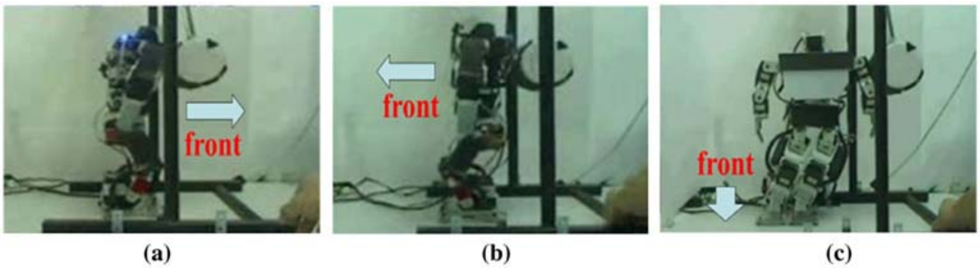

Figure 21. Photographs of the CU-robot resisting an external thrust. (a) The robot is pushed from the front. (b) The robot is pushed from behind. (c) The robot is pushed laterally.

remain balanced on the inclinable platform and to verify the controller's efficiency. The procedure of this experiment is as follows. First, the CU-robot is required to stand on the X–Y two-axis inclinable platform. Next, the platform is tilted forward, backward, or sideward. Finally, the platform stops tilting when the robot's soles slide from the platform. The X–Y two-axis inclinable platform is constructed of three RX-64 motors [24] and the platform's angles of inclination can be measured and recorded from the feedback information of the motors. To compare the effectivity, we evaluate the performance of each experiment using by Equation (10).

$$\eta_t = \left(\frac{T_{on}}{T_{off}} - 100\% \right) \tag{10}$$

in which η_t is the increased stability. T_{on} is the maximum allowed inclination angle when controllers are on; T_{off} is the maximum allowed inclination angle when controllers are off.

5.2.1. The CU-robot is tilted forward and backward

When the CU-robot is tilted forward without any controller, the robot falls down at 5.75 s and the forward inclination angle reaches 8.5° (see the dotted line in Figure 22(a)). On the other hand, the CU-robot with Ankle Control I and Waist Control I can stand stably even when the forward inclination angle reaches around 23.6° (see the solid curve in Figure 22(a) at 22.5 s). It is noted that if the forward inclination angle is larger than 23.6°, the robot may still maintain its standing posture, but the robot's soles slide from the platform.

When the CU-robot is tilted backward without any controller, the robot falls down at 5.75 s when the backward inclination angle reaches −11.3° (see the dotted curve in Figure 22(b)). When Ankle Control I and Waist Control I are applied in this case simultaneously, the CU-robot can stand stably until the backward inclination angle reaches around −22° (see the solid curve in Figure 22(b) at 14 s). It is noted that if the backward inclination angle is smaller than −22°, the robot may still maintain its standing posture, but the robot's soles slide from the platform. By (10), the increased stability of the platform tilted forward is 177.6%; the increased stability of the platform tilted backward is 94.7%.

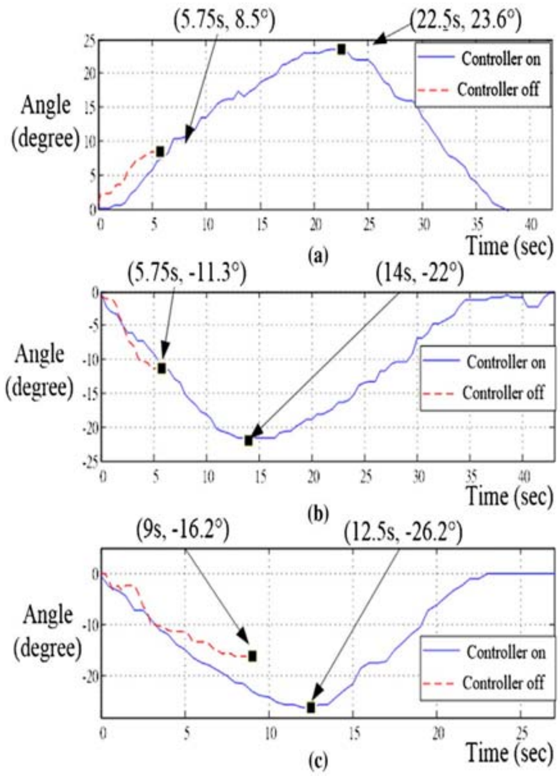

Figure 22. The inclination angle of the platform when CU-robot is tilted (a) forward, (b) backward, and (c) laterally.

5.2.2. The CU-robot is tilted laterally

In this experiment, when the CU-robot is tilted laterally (to the right side) without using any controllers, the robot falls sideways at 9 s when the lateral inclination angle reaches −16.2° (see the dotted curve in Figure 22(c)). When Ankle Control II and Waist Control II are applied simultaneously, the robot can stand stably until the lateral inclination angle reaches around −26.2° (see the solid curve in Figure 22(c) at 12.5 s). It is noted that if the lateral inclination angle is smaller than −26.2°, the robot may still maintain its standing posture, but the robot's soles slide from the platform. The increased stability of the lateral-tilted platform is 61.7%.

5.2.3. The CU-robot is tilted forward and sideways

The robot is required to stand on the platform which is tilted forward and sideways simultaneously, and the forward and sideways inclination angle of the platform is between 0° and 20°. The CU-robot can still maintain its balance without falling down by applying the fuzzy controllers as shown in Figure 23 and the video.[25]

5.3. Walking on a see-saw

In the third experiment, the robot is required to walk on a see-saw which has a spring under each of its two terminals (see Figure (25)). The inclination angle of the see-saw is between −8° and 7.5°. The main purpose of this experiment is to show whether the CU-robot can walk stably on a see-sawing platform and to verify control efficiency during the entire walking procedure. The procedure of this experiment is as follows. First, the CU-robot is required to stand on the center of the see-saw, and then it walks forward to the terminal of the see-saw. Next, the robot walks backward to the other terminal of the see-saw. Finally, the robot walks forward to

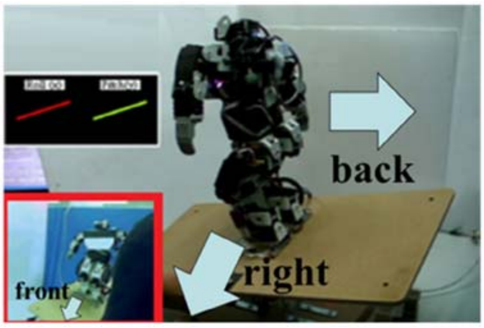

Figure 23. The photographs of the CU-robot standing stably on a platform that is inclinable both forward and sideward.

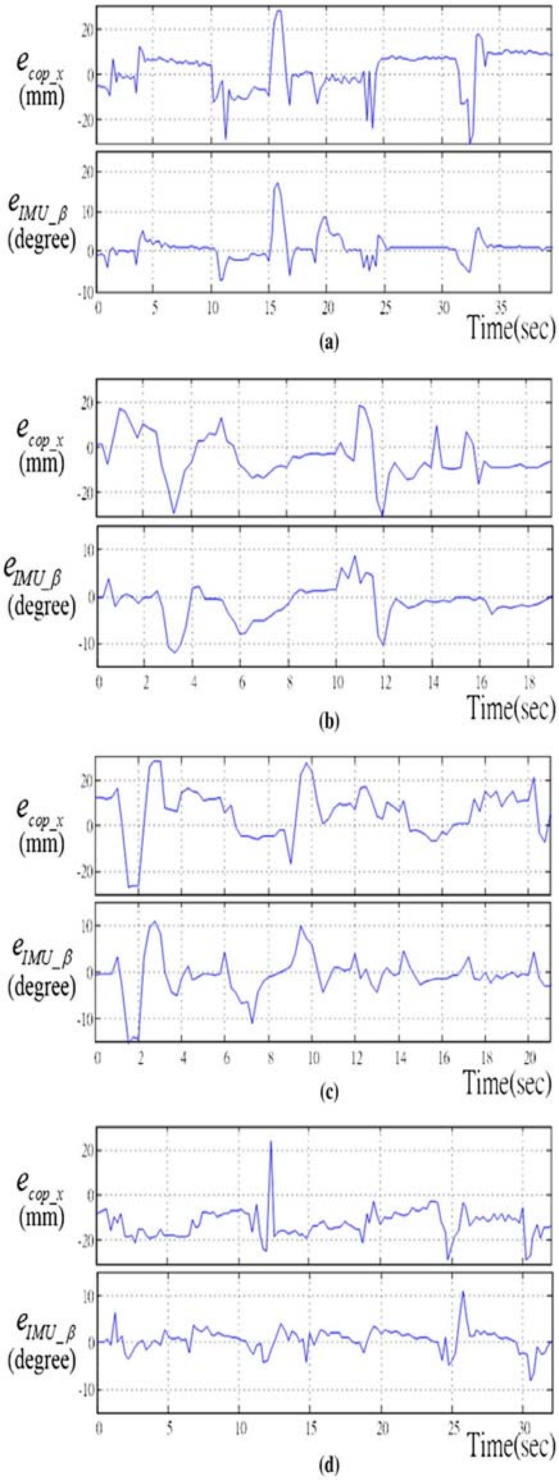

Figure 24. Experimental data when the robot is walking (a) forward and downward, (b) backward and upward, (c) backward and downward, and (d) forward and upward on the see-saw.

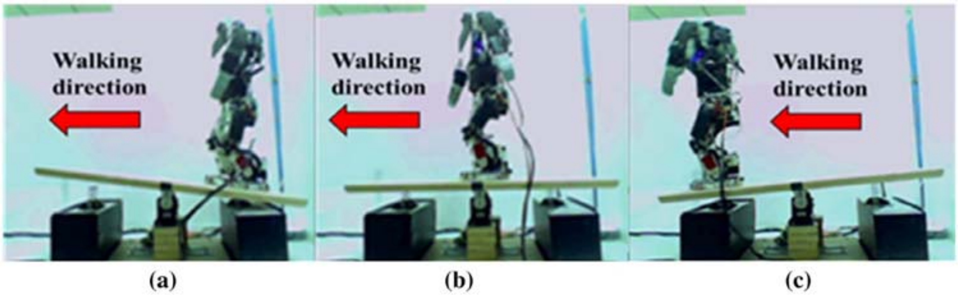

Figure 25. The photographs of the CU-robot walking on a see-saw.

Table 3. The performance of the proposed fuzzy controllers.

Task		Without controller	With controllers	Stability improvement (%)
Thrust resistance	Front	4.1 (kgf cm)	6.2 (kgf cm)	52.1
	Back	3.1 (kgf cm)	4.1 (kgf cm)	32.2
	Sideward	11.9 (kgf cm)	16.5 (kgf cm)	38.6
Standing on a moveable platform	Front	8.5°	23.6°	177
	Back	−11.3°	−22°	94.6
	Sideward	16.2°	26.2°	61.7
	Forward and Sideward	–	Both 20°	–
Walking on a see-saw	Forward and Backward	Fail	Success stepping rate 95%	–

the center of the see-saw. Therefore, four cases, walking forward and downward, walking backward and upward, walking backward and downward, and walking forward and upward, are considered when the robot walks on the see-saw. If the CU-robot walks on the see-saw without any controller, it may fall down due to the see-sawing caused by the two springs. However, by applying Ankle Control I and Waist Control I, the CU-robot can successfully walk on the see-saw as shown in Figure 25 and the video [25]. Figure 24 shows that the stability index e_{cop_x} and e_{IMU_β} are effectively kept within the intervals [−28, 26 mm] and [−15°, 16°], respectively (the stable region of e_{cop_x} is [−50, 50 mm]).

In summary, the performance of the proposed fuzzy controllers in the three tasks is shown in Table 3. When the proposed fuzzy controllers are used, the stability of the CU-robot is increased by at least 32.2 and 61.7% in tasks I and II, respectively. In task III, the CU-robot is required to walk forward and backward on a see-saw. The robot which is not using any controllers can only walk forward two steps before it falls down due to the movement of the see-saw. However, the CU-robot which is using the proposed controllers can walk stably on the see-saw. In this experiment, we performed the walking on a see-saw test 20 times. The robot failed only once during these 20 tests. Therefore, the success rate for the see-saw test is about 95%.

6. Conclusion

In this study, the humanoid robot named 'CU-robot' is required to complete three tasks. The three tasks are resisting a push force from a hammer, standing on a two-axis inclinable platform, and walking on a see-saw. Four fuzzy controllers are designed to adjust the waist and ankle joints of the CU-robot simultaneously using force and IMU sensors as the control inputs. Several experiments are designed and executed to show the successful performance of the CU-robot under various environment disturbances. With the proposed control strategy tests in this study, the stability of the CU-robot is increased by at least 32.2 and 61.7% in tasks I and II, respectively. In addition, the CU-robot walks on a see-saw with a success rate of about 95%.

In summary, the main contribution of this paper is the demonstration of a redesign of the hardware structure of a typical humanoid robot, including a new waist joint with three degrees of freedom and the sensory system, and to propose a complete fuzzy control strategy to overcome more disturbances. Here, we have to admit that the parameters of the fuzzy sets are designed based on our experience in a lot of experiments; how to find a mathematical model or some intelligent algorithm to derive the suitable parameters may be more convincing. In future studies, some sensors such as IR, sonar, or image detection sensors should be placed on the robot in order to obtain more environmental information.

Disclosure statement

No potential conflict of interest was reported by the authors.

Funding

The authors like to thank Ministry of Science and Technology of Taiwan for its support under Contracts NSC102-2221-E-008-085-MY3.

Notes on contributors

Jun-Wei Chang was born in Taipei, Taiwan, in 1985. He received the BS and MS degree from National Formosa University, Yunlin, Taiwan, in 2007 and 2009, respectively. He is currently working toward the PhD degree with the Department of Electrical Engineering, National Central University, Zhongli, Taiwan. His current research interests include fuzzy control, image processing, and intelligent robots.

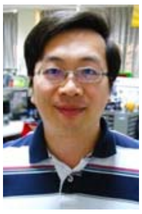

Rong-Jyue Wang received the BS and PhD degree from the Department of Electrical Engineering, National Central University, Chung-Li, Taiwan, ROC, in 1990 and 1995, respectively. He has been an Associate Professor with the Department of Electronic Engineering, National Formosa University, Huwei, Taiwan, ROC, since 2007. His present research interests include robust control, intelligence control, fuzzy control, image recognition and intelligent robots. In recent years, he developed some service robots and performed several intelligent robot R&D projects, the he get over seventy famous robot competition awards.

Che-Han Chang was born in Taipei, Taiwan, in 1988. He received the BS and MS degree from the Department of Electrical Engineering, National Central University, Chung-Li, Taiwan, in 2010 and 2011, respectively. His research interests include robust control, intelligence control, fuzzy control, image recognition and intelligent robots. He is currently working at MiTAC (TYAN) as a senior server firmware engineer, Taipei, Taiwan.

Hao-Gong Chou as born in Taipei, Taiwan, in 1984. He received the BS and MS degree from Chien Hsin University of Science and Technology, Zhongli, Taiwan, in 2007 and 2010, respectively. He is currently working toward the PhD degree with the Department of Electrical Engineering, National Central University, Zhongli, Taiwan. His current research interests include fuzzy control, and field-programmable gate array chip design.

Wen-June Wang received the BS degree in the Department of Control Engineering from National Chiao-Tung University, Hsin-Chu, Taiwan in 1980; and MS degree in the Department of Electrical Engineering from Tatung University, Taipei, Taiwan in 1984. Moreover, he received the PhD degree in the Institute of Electronics from National Chiao-Tung University of Taiwan in 1987. He is presently a Chair Professor of Department of Electrical Engineering. He was the Dean of College of Electrical Engineering and Computer Science, National Central University, Chung-Li City, Taiwan. He was also a Chair Professor and the Dean of the Research and Development Office of National Taipei University of Technology, Taipei, Taiwan in 2007–2009. In 2005–2007, he was the Dean of College of Science and Technology, National Chi-Nan University, Puli, NanTou, Taiwan. Moreover, He obtained the honor of IEEE Fellow in 2008. He has authored or coauthored over 160 refereed journal papers and 160 conference papers in the areas of fuzzy systems and theorems, robust and nonlinear control in large scale systems, and neural networks etc. His most significant contributions are the design of fuzzy systems and the development of robotics. His other research interests include the areas of robot control, neural networks, and pattern recognition etc.

References

[1] Park JH, Chung H. ZMP compensation by online trajectory generation for biped robots. Paper presented at: IEEE International Conference on Systems, Man, and Cybernetics; 1999 Oct 12–15; Tokyo, Japan.

[2] Genci C, Yasuo N, Leonard B, et al. Real time gait generation for autonomous humanoid robots: a case study for walking. Robot. Auton. Syst. 2003;42:107–116.

[3] Kong JS, Lee EH, Lee BH, et al. Study on the real-time walking control of a humanoid robot using fuzzy algorithm. Int. J. Contr. Autom. Syst. 2008;6:551–558.

[4] Taskıran E, Yılmaz M, Koca O, et al. Trajectory generation with natural ZMP references for the biped walking robot SURALP. Paper presented at: IEEE International Conference on Robotics and Automation (ICRA); 2010 May 3–7; Anchorage, AK.

[5] Park JH. Fuzzy-logic zero-moment-point trajectory generation for reduced trunk motions of biped robots. Fuzzy Sets Syst. 2003;134:189–203.

[6] Erbatur K, Okazaki A, Obiya K, et al. A study on the zero moment point measurement for biped walking robots. Paper presented at: 7th International Workshop on Advanced Motion Control; 2002 Jul 3–5; Maribor, Slovenia.

[7] Ferreira JP, Crisostomo MM, Coimbra AP. Human Gait Acquisition and Characterization. IEEE Trans. Instrum. Meas. 2009;58:2979–2988.

[8] Or J. A hybrid CPG–ZMP controller for the real-time balance of a simulated flexible spine humanoid robot. IEEE Transactions on Systems, Man, and Cybernetics, Part C (Applications and Reviews) 2009;39:547–561.

[9] Goswami A. Postural Stability of Biped Robots and the Foot-Rotation Indicator (FRI) Point. The International Journal of Robotics Research 1999;18:523–533.

[10] Popovic MB, Goswami A, Herr H. Ground Reference Points in Legged Locomotion: Definitions, Biological Trajectories and Control Implications. The International Journal of Robotics Research 2005;24:1013–1032.

[11] Loffler K, Gienger M, Pfeiffer F, et al. Sensors and Control Concept of a Biped Robot. IEEE Trans. Industr. Electron. 2004;51:972–980.

[12] Ferreira JP, Crisostomo MM, Coimbra AP, et al. Control of a Biped Robot With Support Vector Regression in Sagittal Plane. IEEE Trans. Instrum. Meas. 2009;58:3167–3176.

[13] Zheng YF, Shen J. Gait synthesis for the SD-2 biped robot to climb sloping surface. IEEE Transactions on Robotics and Automation. 1990;6:86–96.

[14] Rebula J, Canas F, Pratt J, et al. Learning capture points for humanoid push recovery. Paper presented at: IEEE-RAS International Conference on Humanoid Robots; 2007 Nov 29–Dec 1; Pittsburgh, PA.

[15] Hyon SH, Hale JG, Cheng G. Full-body compliant human–humanoid interaction: balancing in the presence of unknown external forces. IEEE Trans. Rob. 2007;23:884–898.

[16] Hauser H, Neumann G, Ijspeert AJ, et al. Biologically inspired kinematic synergies enable linear balance control of a humanoid robot. Biol. Cybern. 2011;104:235–249.

[17] Lee SH, Goswami A. Ground reaction force control at each foot: a momentum-based humanoid balance controller for non-level and non-stationary ground. Paper presented at: IEEE/RSJ International Conference on Intelligent Robots and Systems (IROS); 2010 Oct 18–22; Taipei, Taiwan.

[18] Shih CL, Chiou CJ. The motion control of a statically stable biped robot on an uneven floor. IEEE Transactions on Systems, Man and Cybernetics, Part B (Cybernetics). 1998;28:244–249.

[19] Shahbazi M, Lopes GAD, Babuska R. Observer-based postural balance control for humanoid robot. Paper presented at: IEEE International Conference on Robotics and Biomimetics; 2013 Dec 12–14; Shenzhen, China.

[20] Chen BS, Wu CC, Chen YW. Human walking gait with 11-DOF humanoid robot neural fuzzy networks tracking control. Int. J. Fuzzy Syst. 2013;15:22–35.

[21] RoBoard RB-100. Available from: http://www.roboard.com/.

[22] sparkfun 9 Degrees of Freedom – Razor IMU. Available from: http://www.sparkfun.com/.

[23] ASAKUSAGIKEN Force sensor. Available from: http://www.robotsfx.com/robot/.

[24] ROBOTIS Bioloid robot. Available from: http://www.robotis.com/.

[25] The experiment video of CU-robot. Available from: https://youtu.be/sXjqDt62JTg.